frontiers | Frontiers in Chemistry

TYPE Original Research
PUBLISHED 03 October 2024
DOI 10.3389/fchem.2024.1469520

OPEN ACCESS

EDITED BY
Xiaopeng Han,
Tianjin University, China

REVIEWED BY
Diego González-Flores,
University of Costa Rica, Costa Rica
Feng Hu,
Nanjing University of Aeronautics and Astronautics, China

*CORRESPONDENCE
Changhyun Jin,
z8015026@yonsei.ac.kr
Kyu Hyoung Lee,
khlee2018@yonsei.ac.kr

†These authors have contributed equally to this work contributed to this work

RECEIVED 24 July 2024
ACCEPTED 13 September 2024
PUBLISHED 03 October 2024

CITATION
Kim YH, Lee SY, Ji Y, Lee JH, Kim DW, Lee B, Jin C and Lee KH (2024) Stepwise emergence of CO gas sensing response and selectivity on SnO_2 using C supports and PtO_x decoration. *Front. Chem.* 12:1469520. doi: 10.3389/fchem.2024.1469520

Stepwise emergence of CO gas sensing response and selectivity on SnO_2 using C supports and PtO_x decoration

Yong Hwan Kim[1†], Seung Yong Lee[1†], Yunseong Ji[2†], Jeong Ho Lee[1], Dae Woo Kim[2], Byeongdeok Lee[3], Changhyun Jin[1*] and Kyu Hyoung Lee[1,4*]

[1]Department of Materials Science and Engineering, Yonsei University, Seoul, Republic of Korea, [2]Department of Chemical and Biomolecular Engineering, Yonsei University, Seoul, Republic of Korea, [3]Materials Science and Chemical Engineering Center, Institute for Advanced Engineering, Yongin-si, Republic of Korea, [4]Yonsei-KIST Convergence Research Institute, Seoul, Republic of Korea

Room temperature gas sensing is crucial for practical devices used in indoor environments. Among various materials, metal oxides are commonly used for gas sensing, but their strong insulating properties limit their effectiveness at room temperature. To address this issue, many studies have explored diverse methods such as nanoparticle decoration or conductive support, etc. Here, we report the emergence of gas-sensing functionality at room temperature with improved CO gas selectivity on SnO_2 nanoparticles through sequential steps by using amorphous carbon (a-C) support and PtO_x decoration. The SnO_2 decorated on amorphous carbon shows enhanced gas adsorption compared to inactive gas sensing on SnO_2 decorated carbon support. The higher V_o site of SnO_2 on a-C induces gas adsorption sites, which are related to the higher sp^2 bonding caused by the large density of C defects. The ambiguous gas selectivity of SnO_2/a-C is tailored by PtO_x decoration, which exhibits six values of sensing responses (R_g/R_a or R_a/R_g) under CO gas at room temperature with higher selectivity. Compared to PtO_x/a-C, which shows no response, the enhanced CO gas sensing functionality is attributed to the CO adsorption site on PtO_x-decorated SnO_2 particles. This report not only demonstrates the applicability of CO gas sensing at room temperature but also suggests a strategy for using SnO_2 and carbon compositions in gas sensing devices.

KEYWORDS

SnO_2, gas sensor, CO gases, room temperature, nanocomposites

1 Introduction

The increasing presence of air pollution gases, originating from not only the exhaust systems of combustion engines in heavy industries and vehicles but also from emissions in public places and residential buildings, has raised public awareness of biological health risks (Wang et al., 2018; Hou et al., 2012; Utriainen et al., 2003; Jia et al., 2014; Devaraj et al., 2022; Yamazoe, 2005). In response to this phenomenon, many studies have successfully developed gas sensing devices capable of detecting gases at sensitivities under a few parts per million (ppm) using metal oxide (MO) semiconductors. Consequently, the research trend in advanced gas-sensing materials has focused on improving sensitivity

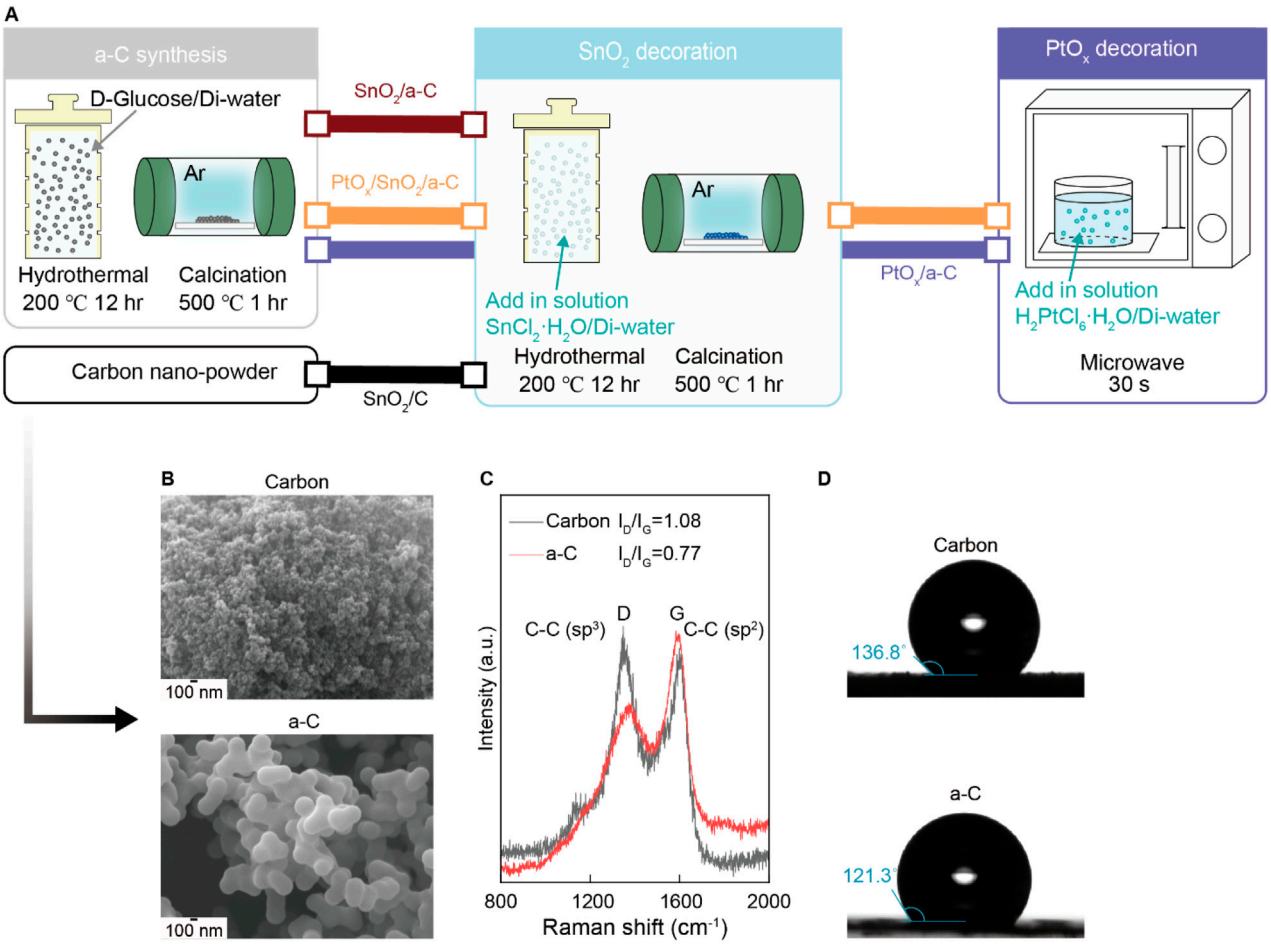

FIGURE 1
(A) Schematic illustration synthesis process of all samples. **(B)** SEM results of Carbon and a-C particles. **(C)** Raman results from Carbon and a-C particles. **(D)** Water contact angle difference of hydrophobic Carbon and a-C particles.

and selectivity, as measured by significant electrical resistance changes before and after analyte gas exposure on the MO surface (Dey, 2018; Franco et al., 2022; Eranna et al., 2024; Simon et al., 2001; Ji et al., 2019; Zakrzewska, 2001; Singh et al., 2021; Chen et al., 2013; Choi et al., 2021; Kim M. Y. et al., 2023; Kim et al., 2023b). This is achieved through various methods such as doping, nano-structuring, and creating heterojunctions. While these developed materials exhibit higher gas sensing performance at high temperatures and require significant electric power, there is a growing demand for room-temperature operational chemiresistor gas sensors. These sensors can be applied to smart mobile devices or IoT applications that monitor toxic gases in indoor environments with low electric power and integrated systems. Despite the increasing market demand for gas sensors that operate at room temperature, metal oxides face challenges due to their large band gaps and the interference caused by the preferred adsorption of hydroxyl groups over target gases on the MO surface (Tang et al., 2022; Srinivasan et al., 2019).

Among the diverse metal oxide (MO) candidates, SnO_2 is one of the most widely used materials for gas sensing applications. SnO_2 is an n-type semiconductor with a wide band gap of more than 3.0 eV, commonly used in gas sensors and catalytic activities due to its unique physical and chemical properties (Sun et al., 2022; Chen and Lou, 2013; Li et al., 2020; Masuda, 2022). Therefore, SnO_2 has been investigated in various forms, such as hydrothermal, sol-gel, electrospinning, and polyol techniques, all of which have demonstrated promising performance (Chen and Lou, 2013; Masuda, 2022; Liu et al., 2023; Tonezzer et al., 2019; Mei et al., 2014; Yin et al., 2019). However, high-temperature operational SnO_2-based gas sensors face challenges due to the strong insulating properties resulting from the large band gap and the adsorption of -OH groups from unavoidable moisture in the air, which interferes with the adsorption of analyte gases on the SnO_2 surface (Tang et al., 2022; Srinivasan et al., 2019; Shah et al., 2022; Duoc et al., 2021). Thus, developing room-temperature operational SnO_2 gas sensors has become a significant goal. To overcome these limitations, many studies have attempted to mix SnO_2 with higher conductivity elements or employ nano-structuring techniques. Nevertheless, the consistently low response at room temperature makes it difficult to determine gas selectivity for these modified materials, leading to a trial-and-error approach in the development of room-temperature operational gas sensing materials.

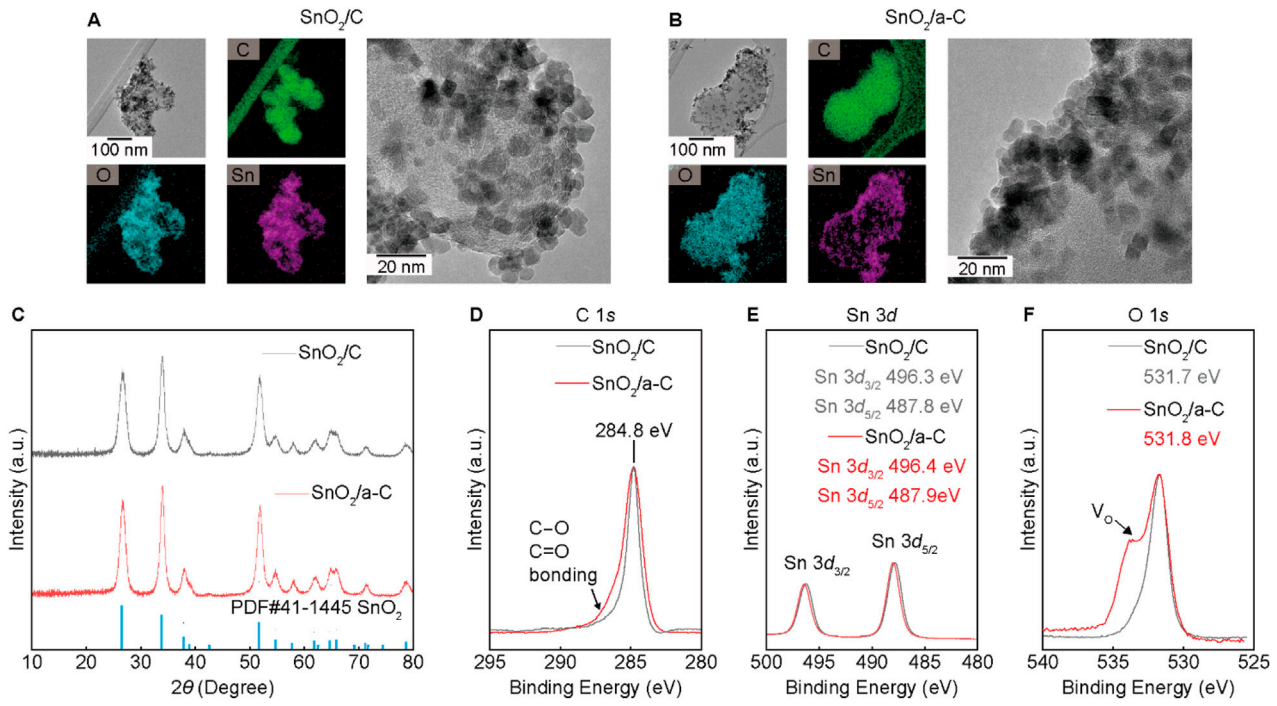

FIGURE 2
SnO_2 on C or a-C particles. **(A, B)** TEM/EDS results of SnO_2/C **(A)** and SnO_2/a-C **(B)**. **(C)** XRD results of SnO_2/C and SnO_2/a-C. **(D–F)** XPS results with composed elements such as C 1*s* **(D)**, Sn 3*d* **(E)**, and O 1*s* **(F)**.

In this report, we sequentially modify SnO_2 to function as a room-temperature gas-sensing material using amorphous carbon (a-C) and PtO_x. We enhance gas adsorption on SnO_2 by using a-C support with a higher concentration of carbon defects, which shows no response in SnO_2/C samples. Subsequently, PtO_x-decorated SnO_2/a-C demonstrates a CO gas selectivity with six of response, which is higher than the response for other gases. This improvement is due to CO adsorption on PtO_x-coated SnO_2 nanoparticles and external charge carrier conduction from PtO_x/SnO_2 to a-C, as opposed to the lack of gas response from PtO_x nanoparticles on a-C. These results suggest a method for modifying MO particles for room-temperature gas sensing using a sequential strategy.

2 Materials and methods

2.1 Material synthesis

SnO_2/a-C. The 34 mmol of D-glucose was dissolved in 170 mL of deionized water and stirred for 30 min. The mixed solution was placed in Teflon inner container and performed hydrothermal synthesis at 200°C for 12 h. After performing centrifuge from hydrothermally synthesized solution were dried in the vacuum oven overnight. The dried powder was conducted in a tube furnace filled with Ar atmosphere at 500°C to obtain the a-C. SnO_2 decoration was again performed via hydrothermal synthesis with $SnCl_4{\cdot}5H_2O$ and a-C. The solution of $SnCl_4{\cdot}5H_2O$ and a-C in deionized water was stirred for 30 min and hydrothermal synthesis was performed at 200°C for 12 h and sequentially dried the centrifuged powder in the vacuum oven overnight. The obtained powder was calcined under an Ar atmosphere at 500°C for 1 h.

SnO_2/C. SnO_2 decoration on carbon was performed via hydrothermal synthesis using $SnCl_4{\cdot}5H_2O$ with nano-sized carbon (Sigma-Aldrich, nano powder carbon <100 nm) under 200°C for 12 h. The solution of $SnCl_4{\cdot}5H_2O$ and carbon nanoparticles in deionized water was stirred for 30 min, and hydrothermal synthesis was performed under 200°C for 12 h. The resulting powder was calcined under an Ar atmosphere at 500°C for 1 h.

PtO_x/SnO_2/a-C and PtO_x/a-C. PtO_x decoration on the SnO_2/a-C or a-C particles was carried out using microwave synthesis for 30 s with $H_2PtCl_6{\bullet}H_2O$ (Sigma-Aldrich, 99.9% trace metals basis) dissolved in deionized water. After drying the synthesized powder overnight in the oven, we obtained the PtO_x/SnO_2/a-C and PtO_x/a-C powder.

2.2 Material characterization

Morphological measurements were conducted by scanning electron microscopy (SEM, JEOL-7800F, JEOL Ltd.) and transmission electron microscopy (TEM, JEM-F200, JEOL Ltd.). The crystal structure characterization was performed using X-ray diffraction (XRD, Smart Lab, Rigaku) with Cu Kα radiation. Chemical bonding states were analyzed via X-ray photoelectron spectroscopy (XPS, K-alpha, Thermo Fisher Scientific Co.) Raman spectroscopy (LabRam Aramis, Horiba Jovin Yvon) was utilized to confirm the carbon vibration mode. The water contact angles for a-C

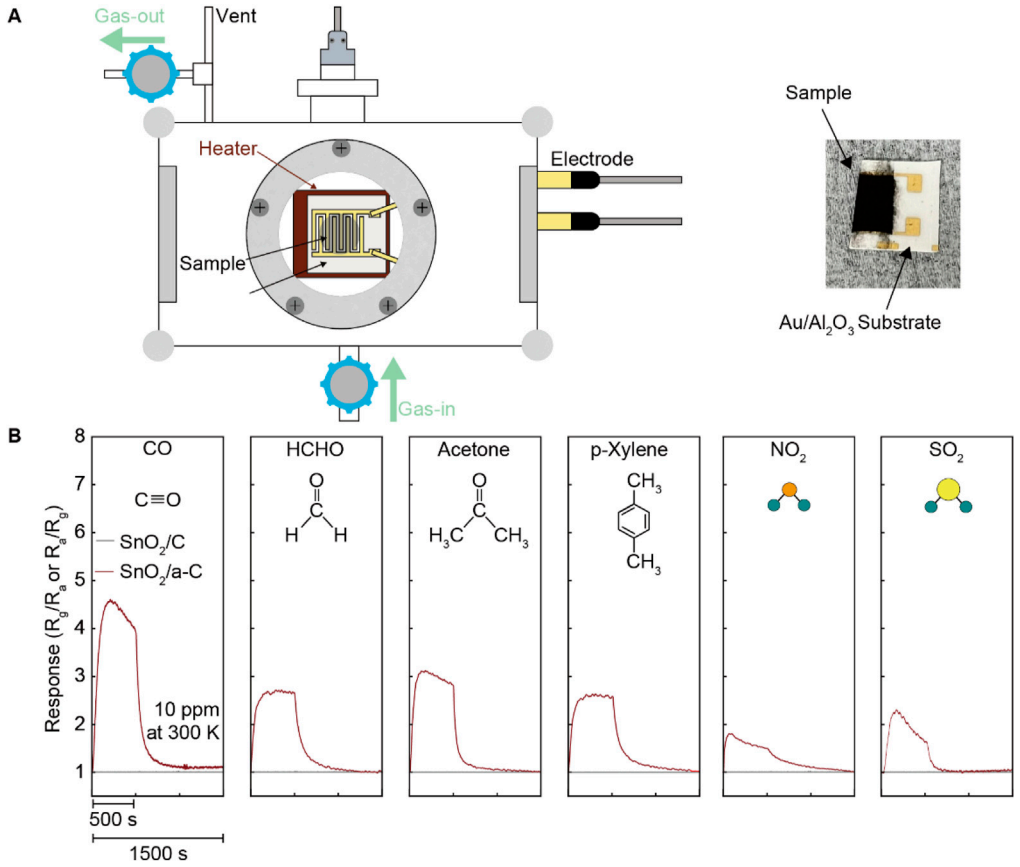

FIGURE 3
Emerged gas sensing functionality on SnO_2/a-C than the SnO_2/C at room temperature. **(A)** Schematically illustrated gas sensing measurement system and photo of SnO_2/a-C coated Au/Al_2O_3 substrate. **(B)** Gas sensing is performed by resistance difference before/after diverse gases exposure such as CO, HCHO, acetone, p-Xylene, NO_2, and SO.

and carbon were measured by Attension Theta Lite (Biolin Scientific).

2.3 Evaluate the gas-sensing performance

A 2-probe electrode configuration was employed for the gas sensing analysis. SnO_2/a-C, SnO_2/a-C, PtO_x/SnO_2/a-C, and PtO_x/a-C properties were uniformly dispersed in ethanol at identical concentrations and subsequently drop-cast onto gold electrodes positioned on an alumina substrate. The gas-sensing performance of the fabricated sensors was evaluated within a custom-built chamber equipped with mass flow controllers, maintaining a fixed flow rate of 500 standard cubic centimeters per minute using air as the carrier gas. The sensors were exposed to target gas concentrations ranging up to 20 ppm for 500 s, followed by a recovery period in air for 1,000 s at a controlled temperature of 30°C. The resistance values in air (R_a) and upon exposure to the target gases (R_g) were recorded, and the sensor response (R_g/R_a) or R_a/R_g) was determined by calculating the ratio of resistance values in ambient air to those under gas exposure conditions Gas sensing measurements were performed for various gases, including Com HCHO, acetone, p-Xylene, Benzene, NO_2, and SO_2.

3 Results

3.1 Emergence of room temperature gas sensing on SnO_2 using amorphous carbon

The emergence of gas adsorption sites on SnO_2 nanoparticles depends on the bonding characteristics of the carbon supports. As shown in the SEM results in Figure 1A, we used various nano-sized carbon and a-C particles for support. The intensity ratio between sp^3 carbon bonding at the D site and sp^2 carbon bonding at the G site, noted as the I_D/I_G ratio in the Raman spectra (Figure 1B), is 0.77 for a-C, indicating a higher G band (sp^2 peak of carbon) bonding in a-C. This implies a higher C vacancy site than in the carbon particles (I_D/I_G = 1.08) and suggests a higher -OH group concentration than in the carbon particles. Consequently, the favorable sp^2 bonding character in a-C results in lower water contact angles compared to the carbon particle surface, as shown in Figure 1C.

SnO_2 nano-particles decorated on carbon supports (SnO_2/C) and a-C (SnO_2/a-C) are shown in the HR-TEM and EDS results (Figures 2A, B). Approximately 10 nm-sized SnO_2 particles are evenly distributed on all Carbon supports. The X-ray diffraction (XRD) results in Figure 2C show the SnO_2 single-phase peaks in all samples. However, the unobservable

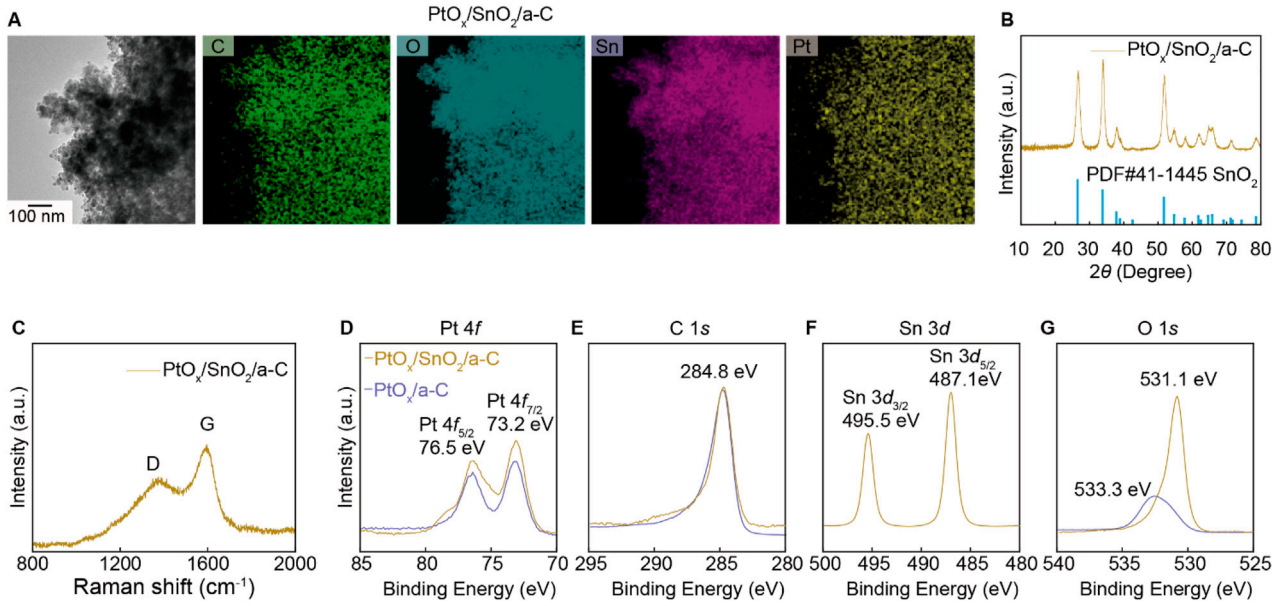

FIGURE 4
Structure analysis of PtO_x decorated on SnO_2/a-C particles. **(A)** TEM/EDS mapping results. **(B)** XRD results. **(C)** Raman results. **(D–G)** XPS results of PtO_x/SnO_2/a-C and PtO_x/a-C with composed elements such as Pt 4*f* **(D)**, C 1*s* **(E)**, Sn 3*d* **(F)**, and O 1*s* **(G)**.

carbon peaks in the XRD results suggest lower crystallinity or an amorphous phase of the carbon supports. The XPS results for SnO_2/C and SnO_2/a-C (Figures 2D–F) demonstrate different chemical bonding characteristics. The carbon XPS results exhibit a larger asymmetric peak in SnO_2/a-C binding energy. The remaining XPS intensity at higher binding energy than 284.8 eV indicates the existence of C-O single bonding or C=O double bonding, suggesting stronger bonding between a-C and Oxygen in SnO_2 particles than in the Carbon supports (Kalish et al., 1999; Chokradjaroen et al., 2021). The Sn 3*d* and O 1*s* results display 496.4 eV for Sn $3d_{3/2}$, 487.9 eV for Sn $3d_{5/2}$, and 531.8 eV for O 1*s* in SnO_2/a-C, whereas SnO_2/C exhibits 496.3 eV for Sn $3d_{3/2}$, 487.8 eV for Sn $3d_{5/2}$, and 531.7 eV for O 1*s*. The higher binding energies of the peak positions indicate that the Sn on decorated SnO_2 nanoparticles maintains the preferred +4 charge state on both the C and a-C supports, consistent with the single-phase SnO_2 XRD pattern. Despite similar maximum peak positions for all samples, the higher Oxygen vacancy (V_O) region compared to the symmetric shape of the O 1s peak is observed in the SnO_2/C sample.

The higher VO density in SnO_2/a-C provides more activated gas adsorption sites compared to SnO_2/C samples. The chemiresistive gas sensing functionality, shown in Figure 3, measured the electrical resistance differences before and after exposure to 10 ppm analyte gases (CO, HCHO, acetone, p-Xylene, NO_2, and SO_2) for SnO_2/C and SnO_2/a-C at room temperature. Unlike SnO_2/C, which shows no significant electrical resistance difference under any of the analyte gases, SnO_2/a-C exhibits a response unit (R_a/R_g, where R_a is the resistance in air and R_g is the resistance under analyte gas) of less than five for all gases. However, SnO_2/a-C shows ambiguous gas selectivity, with a response of 4.5 for CO gas, which is higher compared to less than three for other gases.

3.2 Gas selectivity by PtO_x decoration on the SnO_2/a-C

The ambiguous gas selectivity of SnO_2/a-C particles is modulated by decorating them with PtO_x nanoparticles using hydrothermal synthesis methods. The PtO_x nanoparticles are evenly distributed on the SnO_2/a-C powder, as observed in the HR-TEM/EDS measurements in Figure 4A. The XRD results in Figure 4B show that the few wt% of PtO_x nanoparticles are decorated while maintaining the crystal structure of SnO_2/a-C powder. The Raman spectra of PtO_x/SnO_2/a-C in Figure 4C show a higher sp^2 vibration peak (G) compared to the sp^3 vibration mode peak (D), indicating a higher carbon vacancy on the a-C support. The XPS results for PtO_x/SnO_2/a-C particles in Figures 4D–G show measurements for Pt 4*f*, C 1*s*, Sn 3*d*, and O 1*s*, respectively. Compared to SnO_2/a-C, the PtO_x/SnO_2/a-C samples exhibit a higher binding energy region on a-C, indicating C-O and C=O bonding sites between SnO_2 and a-C. The Sn and O measurements show peaks at 495.5 eV for Sn $3d_{3/2}$, 487.1 eV for Sn $3d_{5/2}$, and 531.1 eV for O 1*s*, respectively. The similar peak positions of the Sn 3*d* peaks indicate a consistent charge state of Sn in SnO_2/a-C samples, remaining in the 4+ valence state. The lower V_O region in the O 1*s* XPS results after PtO_x decoration on SnO_2/a-C suggests complex O bonding with Sn and Pt. The peaks at 73.2 eV for Pt $4f_{7/2}$ and 76.5 eV for Pt $4f_{5/2}$ indicate the fully ionized state of Pt cations as PtO_x on the SnO_2 and a-C support. Furthermore, the oxidation state of Pt in PtO_x/SnO_2/a-C is similar to that in PtO_x/a-C, independent of the matrix

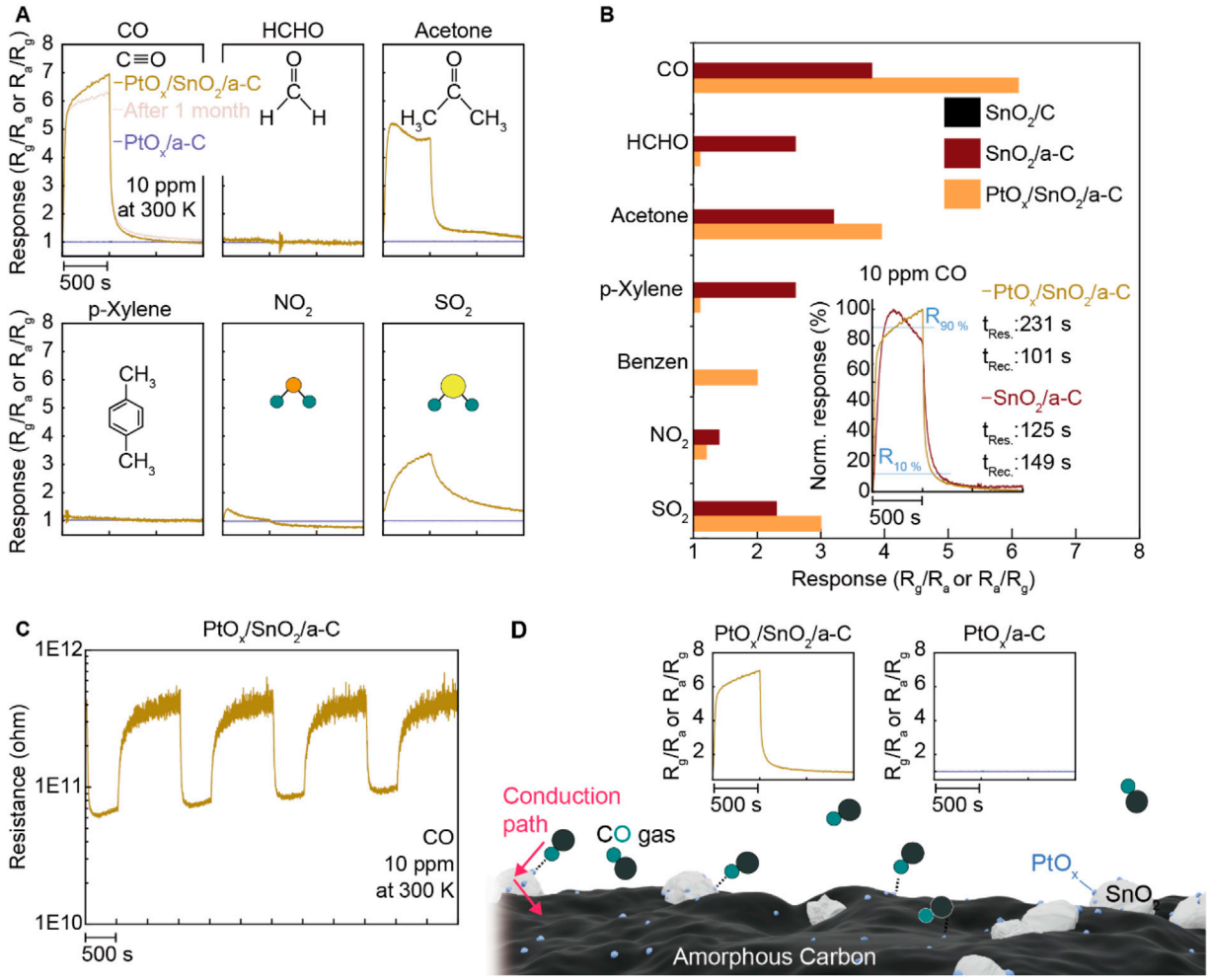

FIGURE 5
Specified gas selectivity on PtO_x/SnO_2/a-C. **(A)** Gas sensing response of PtO_x/SnO_2/a-C and PtO_x/C under diverse gases such as CO, HCHO, acetone, p-Xylene, NO_2, and SO_2. **(B)** Comparison of PtO_x/SnO_2/a-C gas selectivity to SnO_2/C and SnO_2/a-C. The inset plot is the $t_{Res.}$ and $t_{Rec.}$ of PtO_x/SnO_2/a-C and SnO_2/a-C under CO gas. **(C)** The resistance-time plot while operating the gas sensing test. **(D)** Schematic illustrated the emergence of higher CO analyte gas adsorption site on PtO_x/SnO_2/a-C by comparing with none of the gas sensing responses on PtO_x/C.

materials. However, the 533.3 eV O 1s peak, attributed to covalent bonding on the carbon tape, indicates a lower concentration of PtO_x nanoparticles, suggesting that they are physically decorated on the surface without strong chemical bonding with SnO_2 or carbon. The gas selectivity is primarily generated by the PtO_x particles when they are decorated on SnO_2 nanoparticles.

To further investigate the role of PtO_x, we conducted gas-sensing measurements under the same conditions (room temperature, 10 ppm concentration of CO, HCHO, acetone, p-Xylene, NO_2, and SO_2). We also synthesized PtO_x/a-C particles and evaluated their gas-sensing performance. The results, shown in Figure 5A, reveal a gas-sensing response of nearly seven under CO gas. Additionally, the CO gas sensing response of PtO_x/SnO_2/a-C remained consistent 1 month after synthesis, demonstrating higher selectivity for CO compared to other gases (HCHO, acetone, p-Xylene, NO_2, and SO_2). In contrast, PtO_x/a-C powder showed no gas-sensing functionality for all of the tested gases. Comparing the gas selectivity for SnO_2/C, SnO_2/a-C, and PtO_x/SnO_2/a-C, as plotted in Figure 5B, demonstrates that the decorated PtO_x particles impart CO gas selectivity to SnO_2/a-C, which has an activated gas adsorption site. The response and recovery times ($t_{Res.}$ and $t_{Rec.}$) of SnO_2/a-C and PtOx/SnO_2/a-C under 10 ppm of CO gas are shown in the inset. The PtO_x/SnO_2/a-C sample displays a response time of 231 s and a recovery time of 101 s, while the SnO_2/a-C sample exhibits a response time of 125 s and a recovery time of 149 s, respectively. A detailed analysis reveals that PtO_x/SnO_2/a-C demonstrates a faster $t_{Res.}$ than SnO_2/a-C up to 70% of the maximum response, with the $t_{Res.}$ of PtO_x/SnO_2/a-C surpassing that of SnO_2/a-C as it approaches the maximum gas response.

The reversible gas-sensing functionality of PtO_x/SnO_2/a-C during long-term gas-sensing measurements, shown in Figure 5C, demonstrates that PtO_x/SnO_2/a-C is an n-type gas-sensing device and exhibits a stable resistance range of 10^{11}~10^{12} Ω. The higher CO gas selectivity of PtO_x/SnO_2/a-C, compared to the lack of gas response

on PtO_x/a-C, demonstrates that PtO_x on SnO_2 is the primary gas adsorption site, and PtO_x-.SnO_2-a-C provides a sequential external carrier conduction route, as described in Figure 5D.

4 Conclusion

Both a-C and PtO_x provide additional options for enabling gas sensing at room temperature on the SnO_2 semiconductor. Specifically, a-C activates gas sensing functionality with higher gas adsorption at room temperature due to a higher concentration of carbon vacancies, while PtO_x on SnO_2 induces higher CO gas selectivity. These results suggest that this strategy for developing gas sensing materials can be applied not only to SnO_2 but also to other conventional metal oxides with large band gaps, enabling their operation at room temperature.

Data availability statement

The original contributions presented in the study are included in the article/Supplementary Material, further inquiries can be directed to the corresponding authors.

Author contributions

YK: Formal Analysis, Investigation, Methodology, Writing–original draft. SL: Conceptualization, Data curation, Methodology, Writing–original draft, Writing–review and editing. YJ: Formal Analysis, Investigation, Methodology, Writing–original draft. JL: Formal Analysis, Investigation, Writing–original draft. DK: Formal Analysis, Investigation, Writing–original draft. BL: Formal Analysis, Investigation, Writing–original draft. CJ: Conceptualization, Writing–original draft, Writing–review and editing. KL: Conceptualization, Writing–original draft, Writing–review and editing.

Funding

The author(s) declare that financial support was received for the research, authorship, and/or publication of this article. This research was supported by Basic Science Research Program through the National Research Foundation of Korea (NRF) funded by the Ministry of Education (RS-2023-00243422). Kyu Hyoung Lee was supported by Basic Science Research Program through the National Research Foundation of Korea (NRF) funded by the Ministry of Education (NRF-2019R1A6A1A11055660), the Korea government (MSIT). (2022R1A2C2005210) and supported by the Technology Innovation Program ("20013621", Center for Super Critical Material Industrial Technology) funded by the Ministry of Trade, Industry & Energy (MOTIE, South Korea). Yong Hwan Kim was supported by a grant of the Korea Health Technology R&D Project through the Korea Health Industry Development Institute (KHIDI), funded by the Ministry of Health & Welfare, Republic of Korea (HI19C1234). This study was supported by Samsung Electronics Co., Ltd. (IO201216–08204-01).

Conflict of interest

The authors declare that the research was conducted in the absence of any commercial or financial relationships that could be construed as a potential conflict of interest.

Publisher's note

References

Chen, J. S., and Lou, X. W. (2013). SnO_2-Based nanomaterials: synthesis and application in lithium-ion batteries. *Small* 9, 1877–1893. doi:10.1002/smll.201202601

Chen, X., Wong, C. K. Y., Yuan, C. A., and Zhang, G. (2013). Nanowire-based gas sensors. *Sens. Actuators B Chem.* 177, 178–195. doi:10.1016/j.snb.2012.10.134

Choi, M. S., Kim, M. Y., Mirzaei, A., Kim, H.-S., Kim, S.-I., Baek, S.-H., et al. (2021). Selective, sensitive, and stable NO2 gas sensor based on porous ZnO nanosheets. *Appl. Surf. Sci.* 568, 150910. doi:10.1016/j.apsusc.2021.150910

Chokradjaroen, C., Watanabe, H., Ishii, T., and Ishizaki, T. (2021). Simultaneous synthesis of graphite-like and amorphous carbon materials via solution plasma and their evaluation as additive materials for cathode in Li–O_2 battery. *Sci. Rep.* 11, 6261. doi:10.1038/s41598-021-85392-2

Devaraj, M., Rajendran, S., Hoang, T. K. A., and Moscoso, M. S.- (2022). A review on MXene and its nanocomposites for the detection of toxic inorganic gases. *Chemosphere* 302, 134933. doi:10.1016/j.chemosphere.2022.134933

Dey, A. (2018). Semiconductor metal oxide gas sensors: a review. *Mater. Sci. Eng. B* 229, 206–217. doi:10.1016/j.mseb.2017.12.036

Duoc, V. T., Hung, C. M., Nguyen, H., Duy, N. V., Hieu, N. V., and Hoa, N. D. (2021). Room temperature highly toxic NO_2 gas sensors based on rootstock/scion nanowires of SnO_2/ZnO, ZnO/SnO_2, SnO_2/SnO_2 and, ZnO/ZnO. *Sens. Actuators B Chem.* 348, 130652. doi:10.1016/j.snb.2021.130652

Eranna, G., Joshi, B. C., Runthala, D. P., and Gupta, R. P. (2024). Oxide materials for development of integrated gas sensors—a comprehensive review. *Crit. Rev. Solid State Mater. Sci.* 29, 111–188. doi:10.1080/10408430490888977

Franco, M. A., Conti, P. P., Andre, R. S., and Correa, D. S. (2022). A review on chemiresistive ZnO gas sensors. *Sens. Actuators Rep.* 4, 100100. doi:10.1016/j.snr.2022.100100

Hou, C., Li, J., Huo, D., Luo, X., Dong, J., Yang, M., et al. (2012). A portable embedded toxic gas detection device based on a cross-responsive sensor array. *Sens. Actuators B Chem.* 161 (1), 244–250. doi:10.1016/j.snb.2011.10.026

Ji, H., Zeng, W., and Li, Y. (2019). Gas sensing mechanisms of metal oxide semiconductors: a focus review. *Nanoscale* 11, 22664–22684. doi:10.1039/C9NR07699A

Jia, Q., Ji, H., Zhang, Y., Chen, Y. Y., Sun, X., and Jin, Z. (2014). Rapid and selective detection of acetone using hierarchical ZnO gas sensor for hazardous odor markers application. *J. Hazard. Mater.* 276, 262–270. doi:10.1016/j.jhazmat.2014.05.044

Kalish, R., Reznik, A., Nugent, K. W., and Prawer, S. (1999). The nature of damage in ion-implanted and annealed diamond. *Nucl. Instrum. Meth. B* 148, 626–633. doi:10.1016/S0168-583X(98)00857-X

Kim, M. Y., Hwang, J. Y., Mirzaei, A., Choi, S.-W., Kim, S.-I., Kim, H.-S., et al. (2023b). NO_2 gas sensing properties of Ag-functionalized porous ZnO sheets. *Adsorpt. Sci. Technol.* 2023. doi:10.1155/2023/9021169

Kim, M. Y., Lee, S. Y., Kim, J., Park, C. O., Shi, W., Mina, H., et al. (2023a). Generation of nanogaps on porous ZnO sheets via Li-ion implantation: NO_2 gas sensing with ultrafast recovery time. *Sens. Actuators B Chem.* 379, 133283. doi:10.1016/j.snb.2022.133283

Li, B., Zhou, Q., Peng, S., and Liao, Y. (2020). Recent advances of SnO_2 -based sensors for detecting volatile organic compounds. *Front. Chem.* 8, 321. doi:10.3389/fchem.2020.00321

Liu, P., Wang, J., Jin, H., Ge, M., Zhang, F., Wang, C., et al. (2023). SnO_2 mesoporous for highly nanoparticle-based gas sensor sensitive and low concentration formaldehyde detection. *RSC Adv.* 13, 2256–2264. doi:10.1039/d2ra06745e

Masuda, Y. (2022). Recent advances in SnO_2 nanostructure based gas sensors. *Sens. Actuators B Chem.* 364, 131876. doi:10.1016/j.snb.2022.131876

Mei, L., Chen, Y., and Ma, J. (2014). Gas sensing of SnO_2 nanocrystals revisited: developing ultra-sensitive sensors for detecting the H_2S leakage of biogas. *Sci. Rep.* 4, 6028. doi:10.1038/srep06028

Shah, V., Bhaliya, J., Patel, G. M., and Joshi, P. (2022). Room-temperature chemiresistive gas sensing of SnO_2 nanowires: a review. *J. Inorg. Organomet. Polym. Mater.* 32, 741–772. doi:10.1007/s10904-021-02198-5

Simon, I., Bârsan, N., Bauer, M., and Weimar, U. (2001). Micromachined metal oxide gas sensors: opportunities to improve sensor performance. *Sens. Actuators B Chem.* 73 (1), 1–26. doi:10.1016/S0925-4005(00)00639-0

Singh, A. A., Sikarwar, S., Verma, A., and Yadav, B. C. (2021). The recent development of metal oxide heterostructures based gas sensor, their future opportunities and challenges: a review. *Sens. Actuators A Phys.* 332 (1), 113127. doi:10.1016/j.sna.2021.113127

Srinivasan, P., Ezhilan, M., Kulandaisamy, A. J., Babu, K. J., and Rayappan, J. B. B. (2019). Room temperature chemiresistive gas sensors: challenges and strategies—a mini review. *J. Mater. Sci. Mater. Electron.* 30, 15825–15847. doi:10.1007/s10854-019-02025-1

Sun, C., Yang, J., Xu, M., Cui, Y., Ren, W., Zhang, J., et al. (2022). Recent intensification strategies of SnO_2-based photocatalysts: a review. *J. Chem. Eng.* 427, 131564. doi:10.1016/j.cej.2021.131564

Tang, Y., Zhao, Y., and Liu, H. (2022). Room-temperature semiconductor gas sensors: challenges and opportunities. *ACS Sens.* 7, 3582–3597. doi:10.1021/acssensors.2c01142

Tonezzer, M., Izidorod, S. C., Moraes, J. P. A., and Dang, L. T. T. (2019). Improved gas selectivity based on carbon modified SnO_2 nanowires. *Front. Mater.* 6, 277. doi:10.3389/fmats.2019.00277

Utriainen, M., Kärpänoja, E., and Paakkanen, H. (2003). Combining miniaturized ion mobility spectrometer and metal oxide gas sensor for the fast detection of toxic chemical vapors. *Sens. Actuators B Chem.* 93 (1–3), 17–24. doi:10.1016/S0925-4005(03)00337-X

Wang, H., Lustig, W. P., and Li, J. (2018). Sensing and capture of toxic and hazardous gases and vapors by metal–organic frameworks. *Chem. Soc. Rev.* 47, 4729–4756. doi:10.1039/C7CS00885F

Yamazoe, N. (2005). Toward innovations of gas sensor technology. *Sens. Actuators B Chem.* 108 (1–2), 2–14. doi:10.1016/j.snb.2004.12.075

Yin, X. T., Zhou, W. D., Li, J., Wang, Q., Wu, F. Y., Dastan, D., et al. (2019). A highly sensitivity and selectivity Pt-SnO_2 nanoparticles for sensing applications at extremely low level hydrogen gas detection. *J. Alloys Compd.* 805, 229–236. doi:10.1016/j.jallcom.2019.07.081

Zakrzewska, K. (2001). Mixed oxides as gas sensors. *Thin Solid Films* 391, 229–238. doi:10.1016/S0040-6090(01)00987-7